Evolution of olivine fabrics during deep subduction and exhumation of continental crust: Insights from the Yinggelisayi garnet lherzolite, South Altyn, NW China

Guojian Geng[1], Liang Liu[1]*, Haijun Xu[2], Wenqiang Yang[1], Chao Wang[1], Yongsheng Gai[1], Tuo Ma[1], Xin Li[1], Xiaoying Liao[1], Tong Li[1]

[1] State Key Laboratory of Continental Dynamics, Department of Geology, Northwest University, Xi'an, 710069. China;

[2]School of Earth Sciences, China University of Geosciences, Wuhan, 430074, China.

Corresponding author: L. Liu (liuliang@nwu.edu.cn)

Key Points:

- Olivine in the garnet lherzolites exhibited different fabrics during deep subduction and exhumation of the continental crust.
- Olivine fabrics will be dispersed at multi-stage deformation and metamorphism.

Abstract

The different olivine fabrics in ultramafic rocks have been widely used to discuss past tectonic settings, given that the olivine fabrics vary with pressure, temperature and water content. However, there are no researches that whether and how the olivine fabrics transform at different metamorphic stages in a natural rock during the process of deep subduction and exhumation. Yinggelisayi garnet lherzolites from South Altyn have experienced deep continental subduction and exhumation. The garnet lherzolites contain well-preserved residual protolith minerals, and near-peak (M_1), granulite-facies retrograde (M_2), and amphibolite-facies retrograde (M_3) metamorphic mineral assemblages. Olivine grains in M_1 formed at P–T conditions of 2.52–3.08 GPa, 1095–1136°C and low water contents (183–213 ppm H/Si), and showed [010] axes sub-normal to the foliation and [001] axes subparallel to the lineation, which is characteristic of B-type fabric ((010)[001]). Olivine grains in M_2 formed at P–T conditions of 1.31–1.80 GPa, 851–893°C and also low water contents (93–139 ppm H/Si), and exhibited [010] axes sub-normal to the foliation and [100] axes subparallel to the lineation, which is characteristic of A-type fabric ((010)[100]). These observations suggest that olivine fabrics in HP-UHP metamorphosed ultramafic rocks are different in the near-peak and retrograde metamorphic stages, and also that the olivine fabrics can be transformed during deep continental subduction and exhumation. Therefore, the dispersed or no clear olivine fabric probably caused by multi-stage deformation and metamorphism, and the distinct olivine fabrics can also be used as a clue to identify geological processes and better understand metamorphism and deformation during subduction and exhumation.

Plain Language Summary

The Yinggelisayi garnet lherzolites from South Altyn, NW China contain residual protolith minerals, and near-peak (M_1), granulite-facies (M_2) retrograde, and amphibolite-facies (M_3) retrograde metamorphic stages. The olivine porphyroblasts at the near-peak metamorphic stage (M_1) during deep subduction of the continental crust developed the B-type olivine fabric and the fine-grained olivine at retrograde metamorphism (M_2) during exhumation developed the A-type olivine fabric. The distinct olivine fabrics are likely as a clue to indentify the olivine formed at different metamorphic stages.

1 Introduction

Olivine fabrics are described in terms of their relationship to the crystallographic framework (x, y, and z axes), and have an important role in controlling deformational micro-structures (Michibayashi et al., 2016). Based on natural and experimental studies, olivine fabrics are commonly categorized into A-, B-, C-, D-, E-, and AG-type, and have dominant slip systems of (010)[100], (010)[001], (100)[001], {0kl}[100], (001)[100], and (010)[h0l], respectively (Fig. 1; Jung and Karato, 2001; Holtzman et al., 2003; Couvy et al., 2004; Katayama et al., 2004, 2008; Jung et al., 2009a, 2009b, 2013; Ohuchi et al., 2011). Each type of olivine fabric has different formation conditions and geological settings (Xu et al., 2005, 2006; Katayama and Karato, 2006; Jung et al., 2009b; Harigane et al., 2011; Wang et al., 2013a, 2013b; Park and Jung, 2015; Michibayashi et al., 2016). The HP-UHP metamorphosed ultramafic rocks typically have B- and/or C-type olivine fabrics, including samples from the Cima di Gagnone in the Central Alps of Switzerland (Frese et al., 2003; Skemer et al., 2006), Otroy in western Norway (Wang et al., 2013a), northern Qaidam in northwest China (Jung et al., 2013), Zhimafang (Xu et al., 2005, 2006) and Xugou (Wang et al., 2013b) in the Sulu UHP terrane in China, and Songshugou in the Qinling orogen in China (Sun et al., 2019). However, olivine is a common mineral in metamorphosed ultramafic rocks of various stages, and there is seldom of investigation in a natural rock that whether and how the olivine fabrics change at different metamorphic stages during deep subduction and exhumation of continental crust. The Yinggelisayi garnet lherzolites from the South Altyn HP-UHP metamorphic belt have experienced complex metamorphic processes and contain multiple mineral assemblages (Liu et al., 2002; Zhang et al., 2005, 2014; Wang et al., 2011), which are ideal for investigating the evolution of olivine fabrics during deep continental subduction and exhumation. We divide garnet lherzolite into the residual protolith minerals and three metamorphic stages by petrography and geochemistry firstly, and focus on the olivine fabrics at the near-peak and early retrograde metamorphic stages and discuss its geological implication.

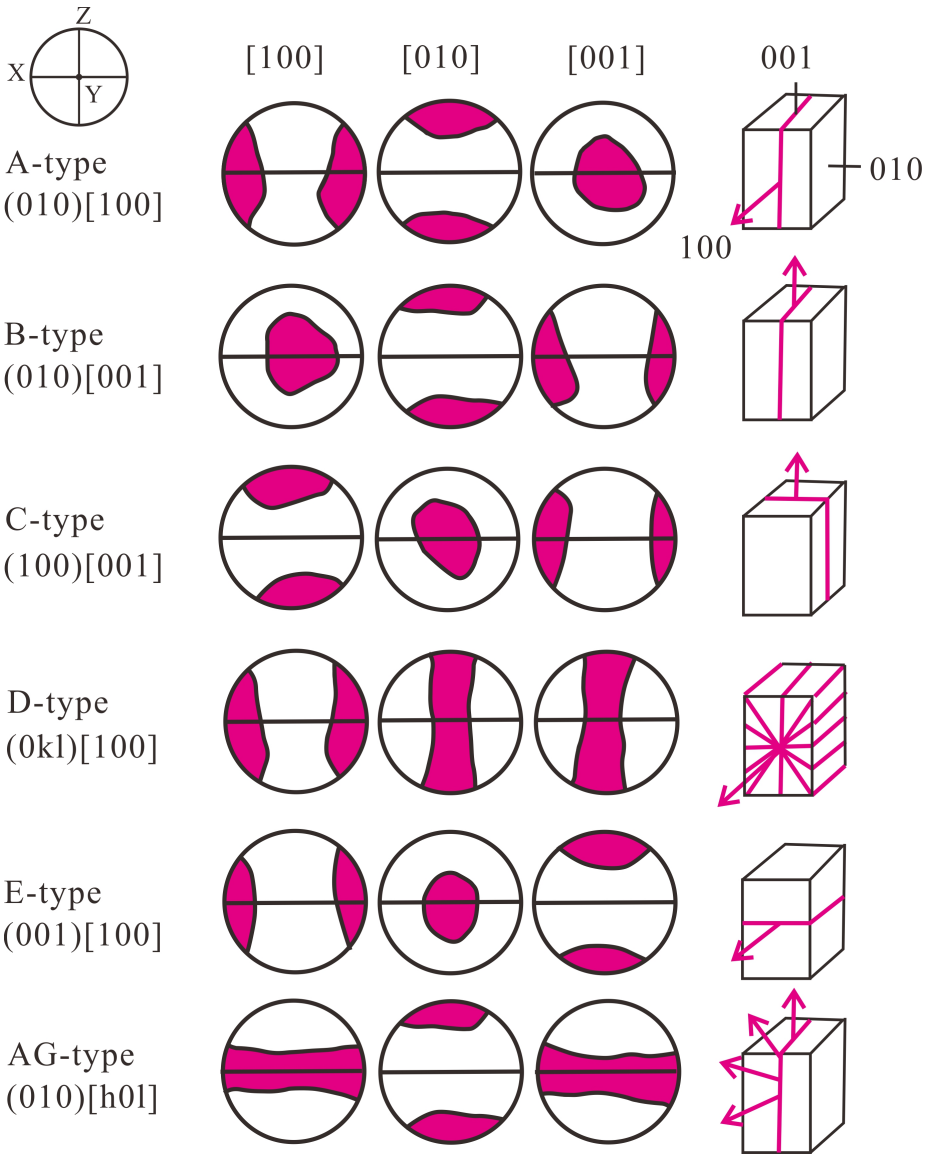

Fig. 1. The six types of olivine fabrics and slip systems (Jung & Karato, 2001; Holtzman et al., 2003; Couvy et al., 2004; Kateyama et al., 2004; Jung et al., 2009a, 2009b; Ohuchi et al., 2011; Michibayashi et al., 2016) shown on lower-hemisphere equal-area projections. X is parallel to the lineation; Y is normal to the lineation and parallel to the foliation; Z is normal to the foliation. The arrows and pink lines in the right-hand column represent the sliding direction and slip plane, respectively.

2 Geological setting

The Altyn Tagh orogen is located along the northern margin of the Qinghai–Tibet Plateau, and is situated between the Tarim Block to the north, and the Qaidam Block and Qilian and Kunlun orogenic belts to the south (Fig. 2a; Wang et al., 2011). Based on structural, geochemical, and geochronological data, the Altyn Tagh orogen can be divided into four units from north to south (Fig. 2b): (1) the Archean North Altyn Terrane, which comprises mainly the granulite-facies Milan Complex and overlying Annanba Group; (2) the Hongliugou–Lapeiquan subduction–collision complex, which includes early Paleozoic ophiolites, pelagic and clastic sedimentary rocks, and HP–LT blueschists and eclogites; (3) the Milanhe–Jinyanshan block, which consists mainly of Meso–Neoproterozoic low-grade metamorphic rocks, schists, limestones, sandstones, mudstones, and thick stromatolites; and (4) the South Altyn subduction–collision complex, which can be further divided into the Jianggalesayi–Danshuiquan–Yinggelisayi HP-UHP metamorphic belt and Apa–Mangya ophiolite complex (Liu et al., 2002, 2012, 2015, 2018; Zhang et al., 2005, 2014; Wang et al., 2011; Gai et al., 2022).

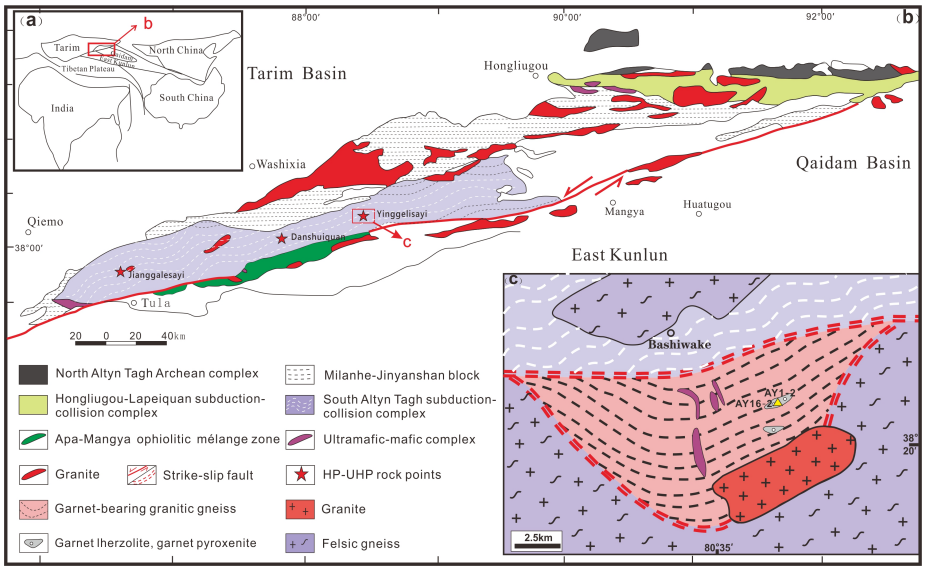

Fig. 2. (a) Location of the Altyn Tagh. (b) Geological map of the Altyn Tagh orogen (modified after Liu et al., 2002). (c) Detailed geological map of the study area showing sampling locations.

The Yinggelisayi area is located in the eastern part of the South Altyn HP-UHP metamorphic belt, near the Altyn Fault (Fig. 2b). Interlayered garnet lherzolite, garnet pyroxenite, and garnet-bearing granitic gneiss (Fig. 3a–b) form a complex lens that is 2500 m long (E-W) and 800 m wide (N-S) (Fig. 2c). The long axis of the lens and lineation in the garnet lherzolites are consistent with the gneissosity that strikes ~280° (Fig. 3c). Previous studies have shown that the Yinggelisayi garnet lherzolites have experienced UHP metamorphism. Liu

et al. (2005) observed clinopyroxene exsolution in garnet from the garnet pyroxenites and proposed that the peak metamorphic conditions were >7 GPa/ ~1000°C. Dong et al. (2019) determined the peak metamorphic pressure of the mafic granulites to be 4–7 GPa based on phase equilibria. Dong et al. (2020) identified pigeonite exsolution along the (401) plane in clinopyroxene in garnetite, which constrains the minimum metamorphic conditions to 6.5–7.0 GPa/ 990°C. Liu et al. (2002) and Wang et al. (2011) used thermobarometry to constrain the metamorphic P–T conditions of the garnet lherzolites to 3.8–5.1 GPa/ 880–970°C, and 4.2–6.0 GPa/920–990°C, respectively. The Yinggelisayi garnet lherzolites also experienced HP granulite- and amphibolite-facies retrograde metamorphism (Liu et al., 2012, 2015; Gai et al., 2022).

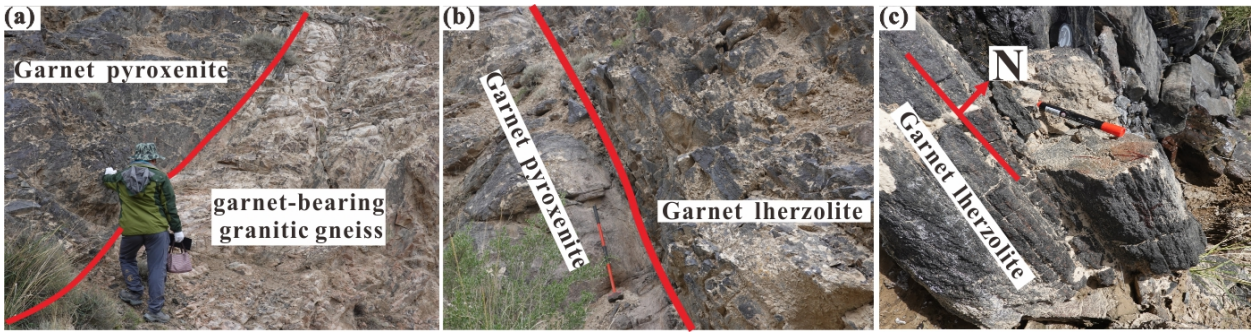

Fig. 3. Photographs of the studied outcrops showing the contact between garnet lherzolite and (a) garnet-bearing granitic gneiss and (b) garnet pyroxene, and (c) garnet lherzolite.

Zircon U–Pb dating of the garnet lherzolites has yielded peak metamorphic ages of *ca.* 501 Ma (Zhang et al., 2005) and *ca.* 498 Ma (Wang et al., 2011), and for felsic granulite of *ca.* 493 Ma (Zhang et al., 2005) and mafic granulite of *ca.* 500 Ma (Dong et al., 2018). These ages for the Yinggelisayi terrane are consistent with those of HP-UHP rocks from the Jianggalesayi and Danshuiquan areas (Liu et al., 2012, 2015; Gai et al., 2022).

3 Methods

Samples were cut normal to the foliation and parallel to the lineation, and made into doubly polished thin-sections. The mineral compositions were determined with an electron microprobe (JXA-8230) at the State Key Laboratory of Continental Dynamics, Northwest University, Xi'an, China. The instrument was operated at an accelerating voltage of 15 kV, a beam current of 10 nA, a beam diameter of 1 m, and with 20 s count times. The natural mineral and synthetic standards were supplied by SPI Company. The trace element compositions of the olivines were determined by laser ablation–inductively coupled plasma–mass spectrometry (LA-ICP-MS) at the State Key Laboratory of Continental Dynamics, Northwest University, Xi'an, China. A laser beam diameter of 43 m and 10 Hz repetition rate were used for the analyses. The data were processed

with ICPMSDataCal software using ^{29}Si as the internal standard (Liu, 2011). The crystallographic preferred orientations (CPO) of olivine was measured by electron backscatter diffraction (EBSD) using a scanning electron microscope (SEM JEOL 6380) at the State Key Laboratory of Geological Processes and Mineral Resources (GPMR), China University of Geosciences, Wuhan, China. The EBSD data were processed using HKL Channel 5 software. The sample surface was inclined at 70° to the incident beam and the EBSD patterns were collected on a phosphor screen. The experimental conditions were as follows: accelerating voltage = 15 kV; working distance ~ 20 mm; spot size = 5.0. The J-index was calculated to estimate the fabric strength of the samples using uncorrelated grain pairs analyzed from the EBSD data (Skemer et al., 2005). The olivine and enstatite water contents were measured by Fourier transform infrared (FTIR; Nicolet 6700) spectroscopy at the China University of Geosciences, Wuhan, China. Unpolarized transmitted light was used to collect the FTIR spectra. Prior to analysis, the samples were made into doubly polished sections with a thickness of 150–250 m, and heated at 120°C for 24 h to eliminate water on the surface of the sections. The water contents were calculated using the calibration method described by Bell et al. (2003) and Hans & Joseph. (2006).

4 Sample descriptions and metamorphic stages

4.1 Petrography and mineral chemistry

The garnet lherzolite consists of olivine (~40%), orthopyroxene (~20%), clinopyroxene (~20%), garnet (~8%), amphibole (~5%), spinel (~2%), and minor accessory minerals such as serpentine and magnesite. The garnet lherzolites have a clear porphyroblastic structure, and garnet, olivine, orthopyroxene, and clinopyroxene porphyroblasts comprise ~30% of the samples. Detail descriptions of each mineral are given below.

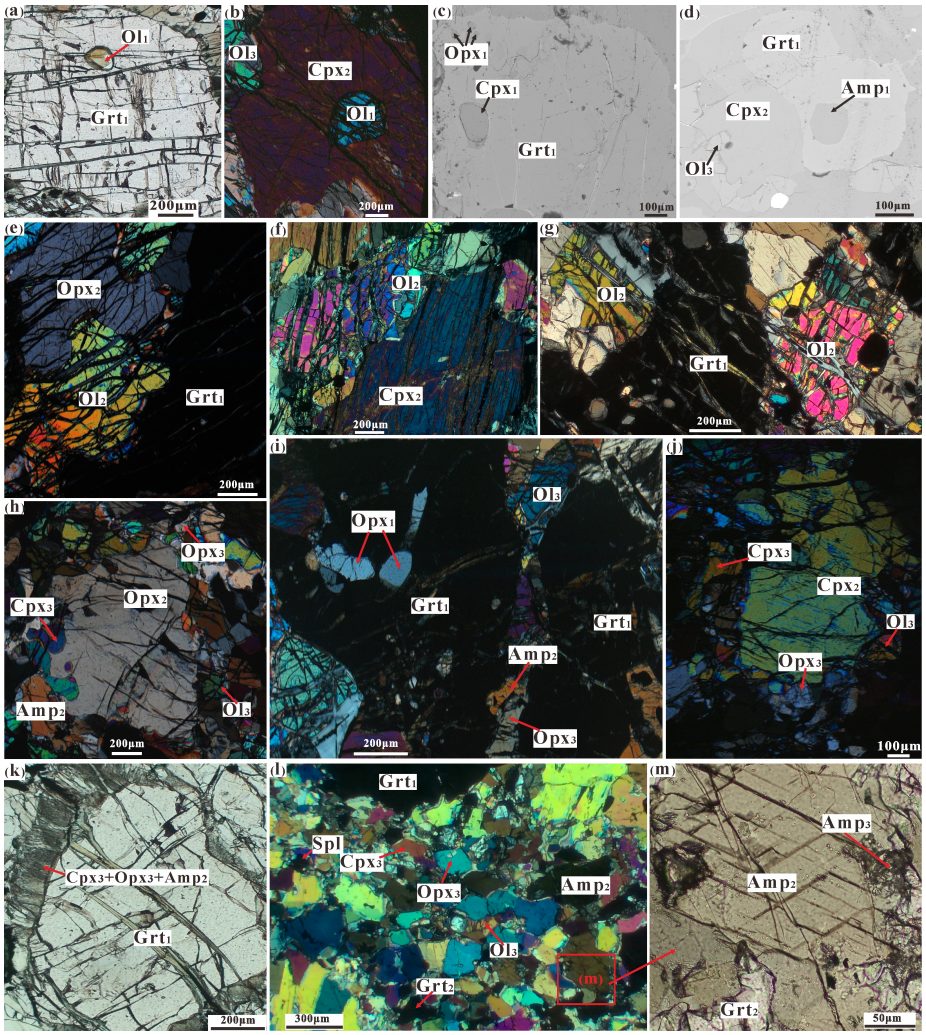

Fig. 4. (a–b, e–m) Photomicrographs and (c–d) back-scattered electron (BSE) images of the studied samples. Abbreviations: olivine: Ol; clinopyroxene: Cpx; orthopyroxene: Opx; garnet: Grt; amphibole: Amp; spinel: Spl.

There are three types of olivine in the samples. The first type (Ol_1) occurs as fine-grained inclusions in garnet and clinopyroxene porphyroblasts (Fig. 4a–b). These inclusions are rounded and crystallized earlier than the coarse-grained garnet and clinopyroxene porphyroblasts. The olivine inclusions have MgO = 40.55–41.25 wt.%, FeO = 18.52–19.97 wt.%, and $Mg^{\#}$ = 79–81. The second type (Ol_2) is coarse-grained olivine porphyroblasts that are ~2 mm in size, which are in equilibrium with coarse-grained garnet, clinopyroxene, and orthopyroxene porphyroblasts (Fig. 4e–g). The coarse-grained olivine contains mesh-like fractures that are mostly infilled with serpentine. These olivines are elongate and

their long axes are oriented E–W, similar to the foliation in the surrounding gneiss. The axial ratios of the coarse-grained olivine are mainly 1.2–2.8, with a maximum of 5.6 (Fig. 5a). The olivine porphyroblasts have MgO = 38.99–40.33 wt.% and FeO = 18.74–21.66 wt.% (Fig. 6a), and Ca = 30.91–311.77 ppm, Ti = 3.33–26.54 ppm (Fig. 6b), Ni = ~700–900 ppm, and Cr = 0.32–33.78 ppm (Fig. 6c). The third type (Ol_3) is fine-grained matrix olivine with diameters of <0.2 mm. The fine-grained matrix olivine grains surround the coarse-grained olivine, garnet, clinopyroxene, and orthopyroxene (Fig. 4b, d, h, and j), and occur in narrow cracks in coarse-grained garnet porphyroblasts (Fig. 4i). This indicates that the matrix olivine crystallized at a late stage. The fine-grained olivine grains also exhibit obvious elongation and a long-axis orientation similar to that of the coarse-grained olivine. The axial ratios of the fine-grained olivine grains are mainly 1.2–3.0, with a maximum of 8.4 (Fig. 5b). The matrix olivine grains have MgO = 38.04–39.06 wt.% and FeO = 20.57–21.85 wt.%. The Ca, Ti, and Cr contents are high and variable (Fig. 6b–c). From the olivine inclusions to the olivine porphyroblasts and to the matrix olivine, MgO contents decrease, FeO contents increase (Fig. 6a), and Ca, Ti, and Cr contents increase (Fig. 6b–c).

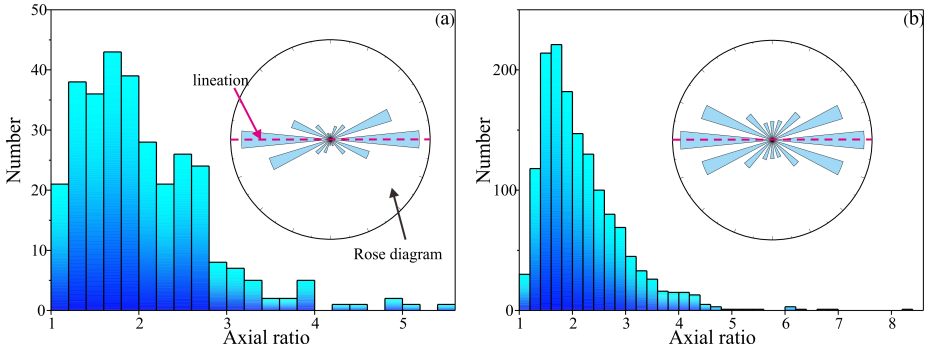

Fig. 5. Histograms of axial ratios and rose diagrams of the (a) coarse-grained olivine porphyroblasts and (b) fine-grained matrix olivine.

The garnet comprises two types, which are coarse-grained porphyroblasts (Grt_1) and fine-grained matrix (Grt_2). The coarse-grained garnets are ~3 mm in size, and contain clinopyroxene, orthopyroxene, and amphibole inclusions (Fig. 4a–b and i). A few coarse-grained garnets are surrounded by intergrown, fine-grained amphibole, clinopyroxene, and orthopyroxene (Fig. 4k). The garnet porphyroblasts have uniform compositions of X_{Prp} = 0.49–0.52, X_{Alm} = 0.32–0.36, X_{Gro} = 0.14–0.15, and X_{Sps} =~ 0.01. The fine-grained matrix garnet grains are <0.5 mm in size and associated with fine-grained clinopyroxene and olivine (Fig. 4l). Compared with the garnet porphyroblasts, Prp contents are slightly lower (0.46–0.49) and Alm contents are slightly higher (0.36–0.37) in the fine-grained garnet matrix (Fig. 7a).

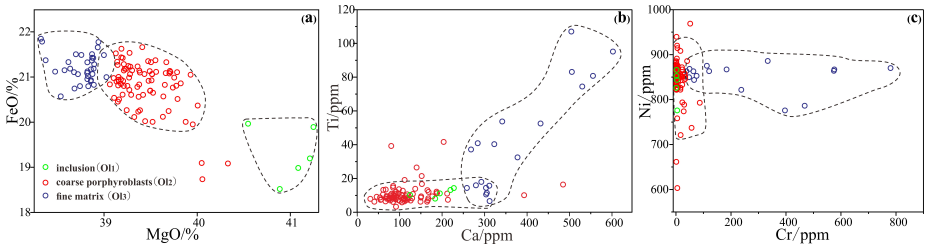

Fig. 6. Plots of olivine (a) MgO–FeO, (b) Ca–Ti, and (c) Cr–Ni contents.

The clinopyroxene inclusions (Cpx_1) in the garnet (Fig. 4b) have relatively high MgO (26.29–32.72 wt.%) and low FeO (2.96–5.10 wt.%) and CaO (5.44–8.88 wt.%) contents, and can be classified as pigeonite (Fig. 7b). Coarse-grained clinopyroxene porphyroblasts (Cpx_2; Fig. 4b, f, and j) have MgO = 15.31–17.25 wt.%, FeO = 4.94–6.80 wt.%, and CaO = 19.64–20.74 wt.%, and can be classified as augite (Fig. 7b). The fine-grained matrix clinopyroxene (Cpx_3; Fig. 4h and j–l) is diopside, and it has the lowest MgO (14.31–15.69 wt.%) and highest CaO (21.68–23.88 wt.%) contents of the three types of clinopyroxene (Fig. 7b).

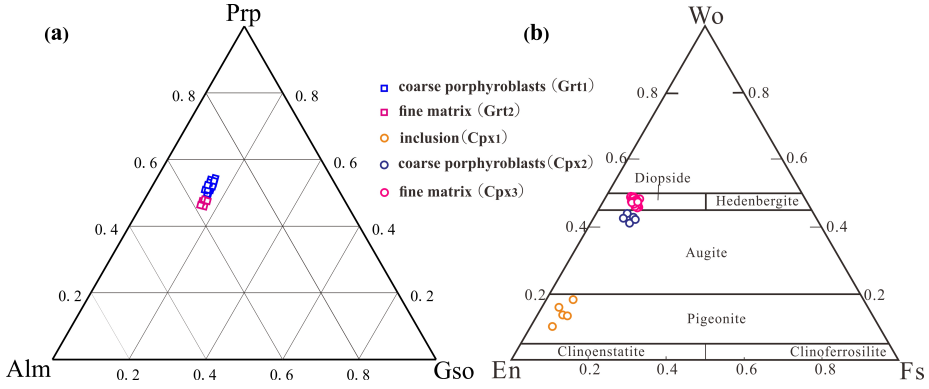

Fig. 7. Mineral compositions of (a) garnet and (b) clinopyroxene.

Similar to the olivine, orthopyroxene occurs as three types: inclusions in coarse-grained garnet (Opx_1; Fig. 4c and i); coarse-grained porphyroblasts (Opx_2; Fig. 4e and h); and fine-grained matrix (Opx_3; Fig. 4h–l). The orthopyroxene inclusions have higher MgO (29.30–29.69 wt.%), lower FeO (10.93–13.38 wt.%), and variable Al_2O_3 (1.36–4.57 wt.%) contents as compared with the other types. MgO contents are slightly lower (28.22–29.04 and 27.67–28.37 wt.%, respectively) and FeO contents are slightly higher (12.24–13.74 and 12.75–13.95 wt.%, respectively) in the coarse-grained orthopyroxene porphyroblasts and fine-grained matrix (Fig. 8a–b).

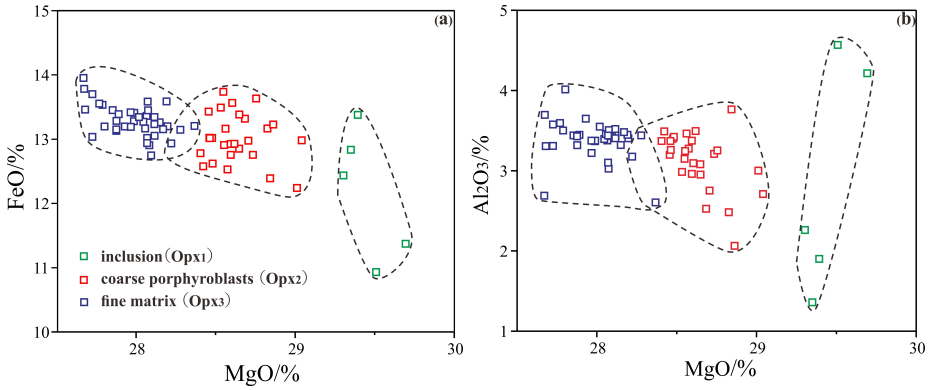

Fig. 8. Plots of MgO versus (a) FeO and (b) Al_2O_3 for orthopyroxene.

The amphibole comprises three types. The first type (Amp_1) occurs as inclusions in coarse-grained garnet (Fig. 4d), and has MgO = 17.05 wt.%, FeO = 8.24 wt.%, and CaO = 9.86 wt.%. The second type (Amp_2) is mostly fine-grained amphibole (Fig. 4h–i, k, and m) and symplectites with clinopyroxene and orthopyroxene that surround the garnet porphyroblasts. Amp_2 has MgO = 14.34–16.76 wt.%, FeO = 6.17–9.22 wt.%, and CaO = 11.18–12.22 wt.%. The third type (Amp_3) surrounds Amp_2 (Fig. 4m) and was formed late.

Spinel is only present in matrix, in association with fine-grained olivine, garnet, clinopyroxene, and orthopyroxene (Fig. 4l). The spinel has Al_2O_3 = 60.03–62.30 wt.%, MgO = 14.04–15.65 wt.%, FeO = 18.50–20.67 wt.%, and Cr_2O_3 = 0.54–0.94 wt.%.

4.2 Metamorphic stages and P-T conditions

Based on the petrography and mineral chemistry of the garnet lherzolites, four mineral assemblages were identified.

(1) The assemblage Ol_1+Opx_1+Cpx_1+Amp_1 is preserved as inclusions in coarse-grained garnet or clinopyroxene porphyroblasts. These minerals probably represent relicts of the protolith. Given that the protolith was a low-pressure ultramafic–mafic igneous rock, the pressure should be <0.8 GPa (Liu et al., 2002). The temperature estimated by Opx–Cpx thermometry (Taylor, 1998) was 1226–1306°C at P = 0.8 GPa.

(2) The assemblage Grt_1+Ol_2+Opx_2+Cpx_2 (M_1) occurs as coarse-grained porphyroblasts that are in equilibrium with each other. We estimated the *P*–*T* conditions by Grt–Cpx barometry (Simakov & Taylor, 2000), Grt–Opx barometry (Nickel & Green, 1985; Taylor, 1998), and Opx–Cpx thermometry (Taylor, 1998; Brey & Kohler, 1990), which yielded P = 2.52–3.08 GPa and T = 1095–1136°C (Table 1).

Table 1. Pressure–temperature estimates for representative samples of garnet lherzolite.

Stage	Simakov & Taylor (2000)	Taylor (1998)	Nickel & Green (1985)	Neill (1981)	Taylor (1998)
	P (Gpa) at T=1100℃		T (℃) at P=2.7Gpa		
	Grt-Cpx	Grt-Opx	Grt-Opx	Cr in Spl	Opx-Cpx
M_1	2.52~2.81	2.64~2.98	2.73~3.08		1121~1136
	P (Gpa) at T=900℃		T (℃) at P=1.5Gpa		
M_2		1.31~1.62	1.42~1.74	1.7-1.8	880~893

(3) The assemblage Grt_2+Ol_3+Opx_3+Cpx_3+Amp_2+Spl (M_2) occurs in the fine-grained matrix and surrounds or is located in fractures in the coarse-grained minerals. Cpx+Opx+Amp intergrowths are only developed around coarse-grained garnet, and their compositions are almost the same as those in the fine-grained matrix. As such, we infer the intergrown and fine-grained matrix minerals represent the earlier retrograde metamorphic stage. The retrograde metamorphic P–T conditions were estimated to be 1.31–1.80 GPa and 851–893°C by Grt–Opx (Nickel & Green, 1985; Taylor, 1998) and Cr-in-spinel (O'Neill, 1981) barometry, and Opx–Cpx thermometry (Taylor, 1998; Brey & Kohler, 1990), which corresponds to the HP retrograde granulite-facies metamorphism.

(4) The final assemblage comprises Amp_3 that crystallized around the matrix amphibole, which suggests that the garnet lherzolites experienced late retrograde amphibolite-facies metamorphism (M_3). Olivine was not formed during this stage. Phase equilibria modeling of garnet lherzolite using THERMOCALC (Yang et al., 2008) showed that the olivine was not significantly affected by the pressure, but olivine became absent at 450–500°C. Given this temperature range, we infer the pressure was <1 GPa based on the amphibolite facies metamorphic stage of Spear (1993).

5. Olivine fabrics of garnet lherzolite

The Yinggelisayi garnet lherzolites contain relict protolith minerals and three metamorphic mineral assemblages. The relict protolith olivine grains are mostly rounded and undeformed, and were insufficient to obtain an ideal olivine fabric. No recrystallized olivine associated with the retrograde amphibolite-facies metamorphism (M_3) was observed. Thus the olivine fabrics in this two stages were not analyzed. The olivine fabrics of the coarse-grained porphyroblasts associated with M_1 and fine-grained olivine associated with M_2 (Fig. 5a–b) were analyzed in detail. We examined the area of olivine grains of >40,000 m^2 for the coarse-grained porphyroblasts (M_1) and create a new subset in Channel 5 program. We examined an area of fine-grained olivine surrounding the garnet, clinopyroxene, and orthopyroxene porphyroblasts of 10,000–30,000 m^2 and extracted the olivine size in this range in Channel 5 program for the fine-grained olivine (M_2) to fabric analysis. The results were that the coarse-grained olivine porphyroblasts exhibited as [010] axes sub-normal to the foliation and [001] axes subparallel to the lineation, which is characteristic of the B-type fabric; and the fine-grained olivine showed as [010] axes sub-normal to the foliation and [100]

axes subparallel to the lineation, which is characteristic of the A-type fabric (Fig. 9).

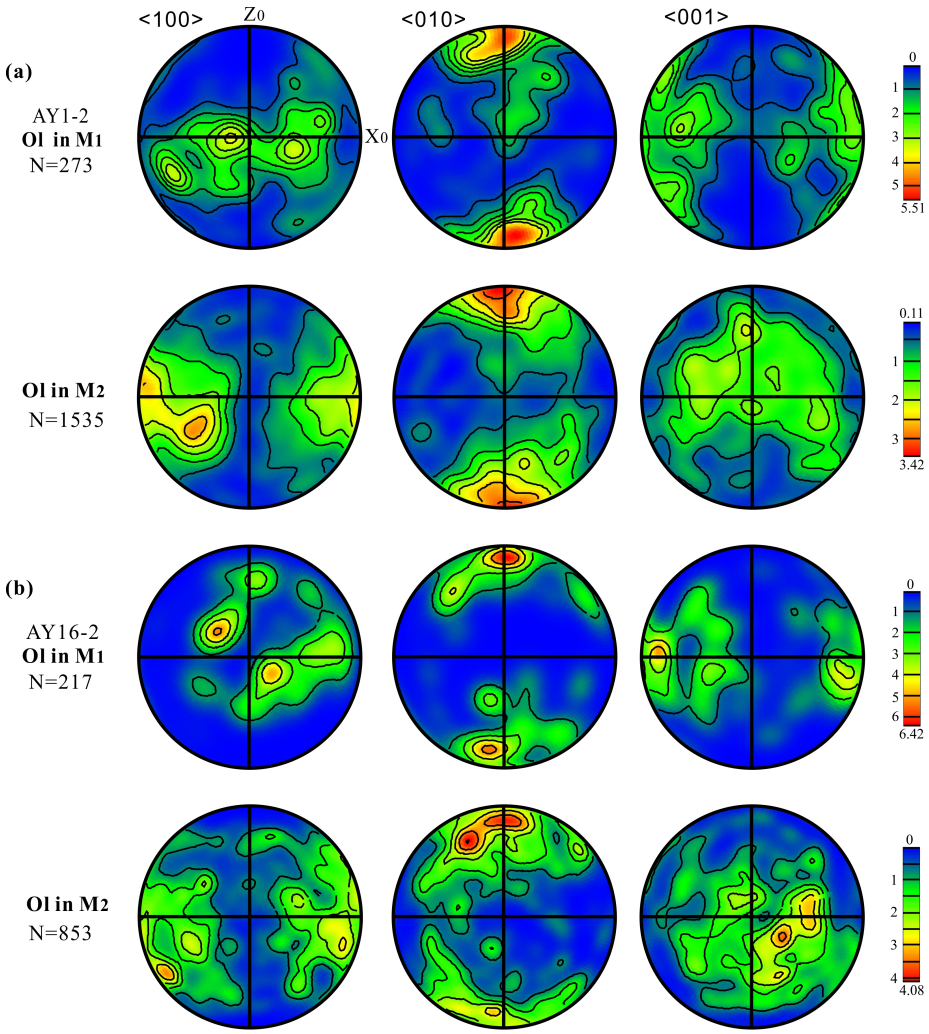

Fig. 9. Lower-hemisphere equal-area projections of poles to olivine. XZ is the sample section, X is the lineation, and Z is normal to the foliation. N is the number of analyzed grains. The color coding represents the data density. A half width of 20° was used to construct the figures.

6. Olivine water contents

Most nominally anhydrous minerals (e.g., olivine and orthopyroxene) contain a small amount of lattice-bound water more or less, which has a significant role in the deformation of such minerals (Jung & Karato, 2001; Wang, 2010). As such, we measured the olivine water contents by FTIR to assess the effects of

water on the olivine fabrics in the garnet lherzolites.

FTIR absorbance spectra of olivine from different stages (M_1 and M_2) are shown in Fig. 10a–b. The wavenumbers 3400–3800 cm^{-1} are shown because this region is dominated by the stretching vibrations of O–H bonds (Paterson, 1982). The dominant absorption peaks are at 3639, 3635, 3624, 3616, 3608, 3574, and 3555 cm^{-1}, and represent structurally bound water in olivine (Bell et al., 2003; Hans & Joseph, 2006). The water contents of the coarse-grained (M_1) and fine-grained (M_2) olivine were calculated using the method of Bell et al. (2003), which yielded values of 183–213 ppm H/Si and 93–139 ppm H/Si, respectively. The coarse- and fine-grained olivine mostly have lower water contents (<200 ppm H/Si), and a few coarse-grained olivine grains have higher water contents (~278 ppm H/Si), perhaps due to later serpentinization or the presence of amphibole inclusions. The FTIR peaks at 3699, 3688, 3683 cm^{-1} and 3677, 3663, 3662 cm^{-1} can be attributed to serpentine (Wang et al., 2007; Jung, 2009b) and amphibole (Hans & Joseph, 2006; Wang et al., 2007), respectively.

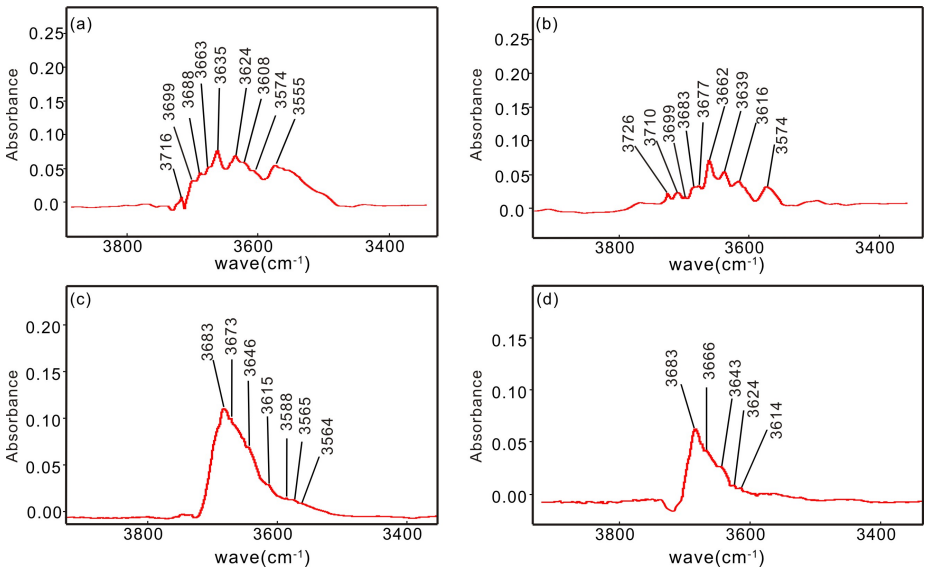

Fig. 10. Representative FTIR spectra of olivine and orthopyroxene. (a) Coarse-grained olivine with inclusions (sample AY1-2). (b) Fine-grained olivine without inclusions or serpentinization (sample AY1-2). (c) Coarse-grained orthopyroxene (sample AY1-2). (d) Fine-grained orthopyroxene (sample AY16-2).

Jung et al. (2013) suggested that the water contents measured in olivine cannot represent the actual water content, because olivine has a high rate of H diffusion (Kohlstedt & Mackwell, 1998), and water can be readily lost or added. Therefore, we also calculated the water contents of the orthopyroxene (Fig. 10c–d), because orthopyroxene has a lower rate of H diffusion than olivine (Mackwell & Kohlstedt, 1990), and may more accurately record the water content of the garnet lherzolites. The coarse- and fine-grained orthopyroxene grains have wa-

ter contents of 21–143 ppm H/Si, which also indicate that the garnet lherzolite cystallized under low water condition at M_1 and M_2 stages.

7. Discussion

7.1 Metamorphic evolution

Based on the petrography and estimated *P*–*T* conditions, residual protolith minerals (i.e., inclusions) and three metamorphic stages were recognized in the Yinggelisayi garnet lherzolites. Previous studies of the metamorphism of the garnet peridotites, garnet pyroxenites, and garnetites have identified peak pressures of up to 4–7 GPa, indicating that the Yinggelisayi terrane was subducted to a depth of ~200 km (Liu et al., 2002, 2005; Dong et al., 2018, 2019, 2020). However, the pressures obtained from the Grt–Opx thermobarometer for the garnet lherzolites vary in different studies. Liu et al. (2002) and Wang et al. (2011) obtained pressures of 4–6 GPa, and Zhang et al. (2005) and Li et al. (2013) obtained pressures of 1.7–2.7 GPa. In the present study, we obtained pressures of 2.52–3.08 GPa. The pressures obtained by Grt–Opx thermobarometry exhibit a negative correlation with the Al_2O_3 contents of orthopyroxene (Wu & Zhao, 2011; Li et al., 2018). The pressures of 4.2–6.0 GPa estimated for the garnet lherzolites by Wang et al. (2011) were based on Grt–Opx barometry, where the Al_2O_3 contents of the orthopyroxene were 0.30–0.66 wt.%. In our samples, the Al_2O_3 contents of the orthopyroxene porphyroblasts are all >2.71 wt.%, much higher than those reported by Wang et al. (2011). This may be due to differences in the sampling locations, or because our samples did not record the peak pressure, given their rapid exhumation. Therefore, the coarse-grained minerals in our samples may represent the near-peak metamorphic stage. The peak metamorphism occurred at *ca.* 500 Ma (Zhang et al., 2005; Wang et al., 2011; Dong et al., 2018). Subsequently, the garnet lherzolites underwent HP retrograde granulite-facies metamorphism. During this stage, the garnet and clinopyroxene retrograded into Cpx_3+Opx_3+Amp_2 symplectites with a vermicular texture around the coarse-grained garnet, and fine-grained olivine, garnet, clinopyroxene, and orthopyroxene recrystallized around the coarse-grained porphyroblasts (e.g., garnet and clinopyroxene). The age of this retrograde metamorphic stage is *ca.* 480 Ma (Zhang et al., 2005; Dong et al., 2018; Gai et al., 2022). The steep P–*T* path, near-isothermal decompression (Fig. 11), and ~20 Myr elapsed indicate that the garnet lherzolites underwent rapid exhumation during the near-peak to HP granulite-facies metamorphism. Finally, the garnet lherzolites underwent amphibolite-facies metamorphism and Amp_3 crystallized around the fine-grained amphibole (Amp_2). There are several stages of granitic intrusions in the South Altyn complex, and their ages (426–385 Ma) are interpreted to be the age of the retrograde amphibolite-facies metamorphism (Liu et al., 2015).

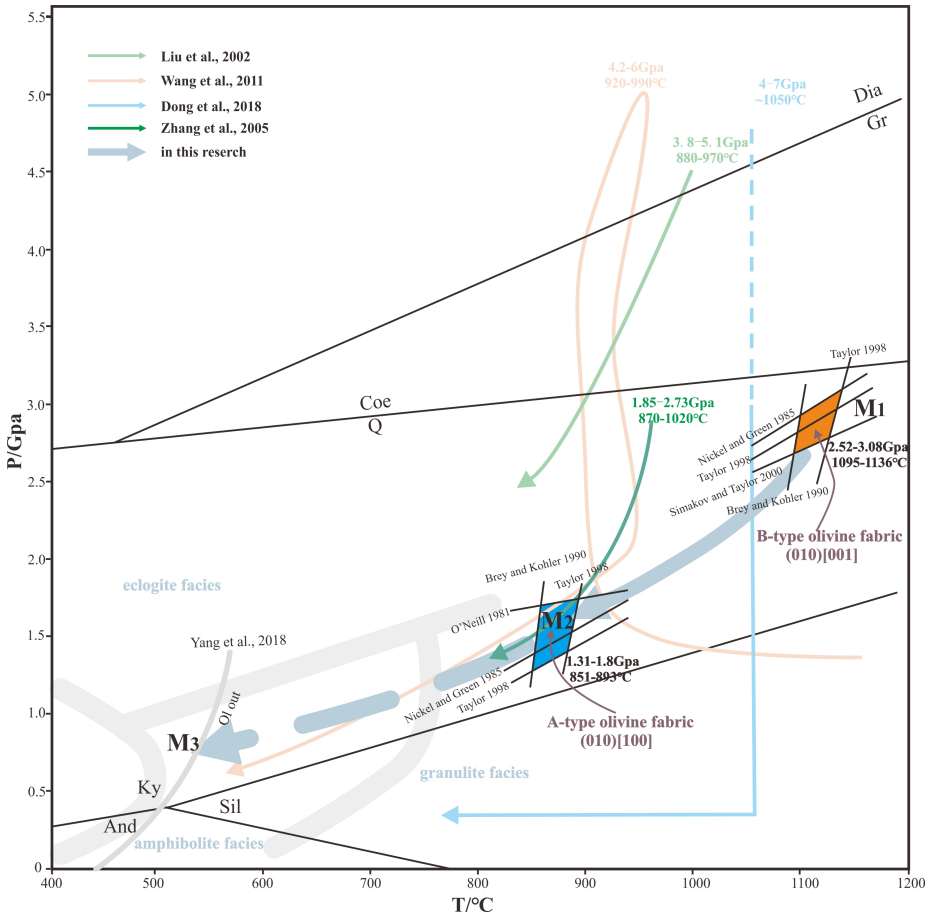

Fig. 11. Summary of published P–T paths for the Yinggelisayi area. The metamorphic facies and conditions are from Spear (1993). The Ol-out line is based on phase equilibria modeling of garnet lherzolite using THERMOCALC (Yang et al., 2008).

7.2 Olivine fabrics in the Yinggelisayi garnet lherzolites during deep subduction and exhumation

Experimental studies have shown that A-type olivine fabric transform to B-type fabric when the pressure increases (Couvy et al., 2004; Ohuchi et al., 2011). Jung et al. (2009a) showed that A-type olivine fabric changes to B-type fabric in the pressure range of 2.5–3.1 GPa. These experimental results suggest that the olivine fabrics varies with pressure. Although, there A-, B-, C-type olivine fabrics developed in the same HP-UHP terrane or belt (Wang et al., 2013a; Sun et al., 2019), these different fabrics are from different rocks and sampling location. And we discuss the olivine fabrics at different metamorphic stages in a natural rock, which is more directly indicating that the variation of olivine

fabrics during the deep subduction and exhumation.

In the studied samples, the coarse-grained olivine porphyroblasts developed B-type fabric and the fine-grained olivine exhibited A-type fabric. The B-type olivine fabric developed in HP-UHP metamorphic rocks from the Cima di Gagnone in the Central Alps of Switzerland (Skemer et al., 2006), Otroy in western Norway (Wang et al., 2013a), and Songshugou in the Qinling orogen of China (Sun et al., 2019), as well as in some HP-UHP experimental studies (Jung et al., 2009a; Ohuchi et al., 2011). Our samples are also HP-UHP metamorphic rocks, which experienced conditions suitable for formation of the B-type olivine fabric. Moreover, the pressure estimated for the near-peak metamorphism (2.52–3.08 GPa) is consistent with the experimental results for the development of the B-type olivine fabric (2.5–3.1 GPa) obtained by Jung et al. (2009a). Although water can also promote the formation of the B-type olivine fabric (Mizukami et al., 2004; Katayama & Karato, 2006; Sun et al., 2019), the lower water contents of this studied olivine grains indicate that water did not have an important role in the formation of the B-type olivine fabric. Therefore, the pressure was probably the main factor that caused the formation of the B-type olivine fabric. The A-type olivine fabric is generally formed in an extensional tectonic setting (Jung et al., 2009b), but also occurs occasionally with B- and/or C-type fabrics in HP-UHP terranes. Previous studies have suggested that the pressure might prevent the formation of the A-type olivine fabric (Durinck et al., 2005; Wang et al., 2007; Jung et al., 2009b). As such, the A-type olivine fabrics observed in HP-UHP terranes have mostly been interpreted as residual fabrics that existed prior to subduction (Wang et al., 2013; Sun et al., 2019). However, the A-type fabric of the fine-grained olivine in the present study is obviously not a relict fabric, but formed during exhumation of the retrograde metamorphic stage. Therefore, we conclude that the coarse-grained olivine porphyroblasts developed the B-type olivine fabric because of the HP-UHP and low-water metamorphic conditions, and the fine-grained olivine showed the A-type olivine fabric due to the pressure decrease during retrograde metamorphism and exhumation.

Therefore, distinct olivine fabrics form under different deformation and metamorphic conditions during deep continental subduction and exhumation. As such, the different olivine fabrics developed in a sample could reflect the deformation stages and may also be used as a clue to identify the different geological stages or tectonic environment.

7.3 AG-like olivine fabric

The AG-type olivine fabric is different from the other olivine fabrics, and forms via least two slip systems: (010)[100] and (010)[001] (Fig. 1). Although the AG-type olivine fabric is relatively uncommon worldwide, it has been reported from many localities in various tectonic settings (Ben et al., 2001; Michibayashi & Mainprice, 2004; Bascou et al., 2008; Tommasi et al., 2008; Muramoto et al., 2011). The AG-type fabric has been explained by the co-existence of an oriented melt (Holtzman et al., 2003; Tommasi, 2006), simultaneous activation of [100] and [001] slip directions (Tommasi et al., 2000), and [010] axial compression

(Harigane et al., 2011). However, the coarse-grained (M_1) and fine-grained (M_2) olivine grains of the present study have [010] axes normal to the foliation and [100] and [001] axes as a girdle parallel to the foliation, similar to the AG-type olivine fabric (Fig. 12). This AG-like fabric developed from a mixture of B- and A-type fabrics that formed at different metamorphic stages which is quite different from the real AG-type fabric proposed by predecessors. Therefore, when encountering the AG-like fabric or the crystalline axes girdled distribution (like D-type fabric) or there are several areas in stereographic projection (or no clear fabric), we should carefully consider whether it is a mixture of different geological stages, otherwise, maybe neglect many geological processes.

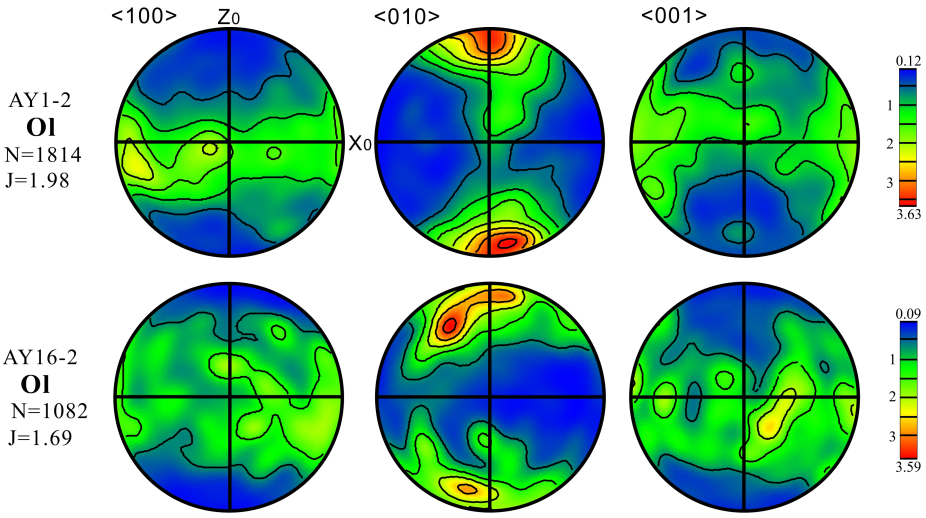

Fig. 12. Lower-hemisphere equal-area projections of the olivine fabrics in the garnet lherzolites. XZ is the sample section, X is the lineation, and Z is normal to the foliation. N is the number of analyzed olivine grains. J-index is the strength of the olivine fabric.

8 Conclusions

(1) The Yinggelisayi garnet lherzolites from South Altyn contain residual protolith minerals, and near-peak (M_1), granulite-facies (M_2) retrograde, and amphibolite-facies (M_3) retrograde metamorphic mineral assemblages. The estimated P–T conditions of M_1 and M_2 are 2.52–3.08 GPa/1095–1136°C, and 1.31–1.80 GPa /851–893°C, respectively.

(2) The coarse-grained olivine porphyroblasts crystallized at the near-peak metamorphic stage (M_1) during deep subduction of the continental crust and developed the B-type olivine fabric. The fine-grained olivine around the porphyroblasts recrystallized in decompression and retrograde metamorphism (M_2) during exhumation, and developed the A-type olivine fabric.

(3) Distinct olivine fabrics developed during different stages of metamorphism

and deformation, and the study of olivine fabric combining with metamorphic stages makes us better understand the metamorphism and deformation evolution history during deep subduction and exhumation of continental crust.

Declaration of competing interests

The authors declare that they have no known competing financial interests or personal relationships that could have appeared to influence the work reported in this paper.

Acknowledgments

This research was financially supported by the National Natural Science Foundation of China (Grants 42030307, 41972054, and 41902051).

References

Bascou, J., Delpech, G., Vauchez, A., Moine, B.N., Cottin, J.Y., & Barruol, G. (2008). An integrated study of microstructural, geochemical, and seismic properties of the lithospheric mantle above the Lerguelen plume (Indian Ocean). *Geochemistry. Geophysics. Geosystem*, 9, Q04036. doi:10.1029/2007GC001879

Bell, D. R., Rossman, G. R., Maldener, J., Endisch, D., & Rauch, F. (2003). Hydroxide in olivine: a quantitative determination of the absolute amount and calibration of the IR spectrum. *Journal of Geophysical Research: Solid Earth*, 108, 1-9.

Ben, I. W., Barruol, G., & Mainprince, D. (2001). The Kaapvaal craton seismic anisotropy petrophysical analyses of upper mantle kimberlite nodules. *Geophysical Research Letters*, 28, 2497-2500.

Brey, G.P. & Köhler, T. (1990). Geothermometry in four–phase lherzolites. II. New thermobarometers, and practical assessment of existing thermobarometers. *Journal of Petrology*, 31, 1353-1378.

Couvy, H., Frost, D.J., Heidelbach, F., Nyilas, K., Ungar, T., Mackwell, S., & Corfier, P. (2004). Shear deformation experiments of forsterite at 11Gpa and 1400 ℃ in the multianvil apparatus. *European Journal of Mineralogy*, 16, 877-889.

Dong, J., Wei, C. J., Chen, J., & Zhang, J. X. (2020). P-T-t Path of Garnetites in South Altyn Tagh, West China: A Complete Record of the Ultradeep Subduction and Exhumation of Continental Crust. *Journal of Geophysical Research: Solid Earth*, 125. e2019JB018881. https://doi.org/10.1029/2019JB018881

Dong, J., Wei, C. J., Clarke, G. L., & Zhang, J. X. (2018). Metamorphic Evolution During Deep Subduction and Exhumation of Continental Crust: Insights from Felsic Granulites in South Altyn Tagh, West China. *Journal of Petrology*, 59(10), 1965-1990.

Dong, J., Wei, C. J., & Zhang, J. X. (2019). Ultra high temperature metamorphism of mafic granulites from South Altyn Oregen, West China: A result

from the rapid exhumation of deeply subducted continental crust. *Journal of Metamorphic Geology*, 37, 315-338.

Durinck, J., Legris, A., & Cordier, P. (2005). Pressure sensitivity of olivine slip systems: first-principle calculations of generalised stacking faults. *Physics and Chemistry of Minerals*, 32, 646-654.

Frese, K., Trommsdorff, V., & Kunze, K. (2003). Olivine [100] normal to foliation: lattice preferred orientation in prograde garnet peridotite formed at high H2O activity, Cima di Gagnone (Central Alps). *Contributions to Mineralogy and Petrology*, 145, 75–86.

Gai, Y. S., Liu, L., Zhang, G. W., Wang, C., Liao, X. Y., Yang, W. Q., Kang, L., Ma, T., & Cao, Y. T. (2022). Differential exhumation of ultrahigh-pressure metamorphic terranes: A case study from South Altyn Tagh, western China. *Gondwana Research*, 104, 236-251. https://doi.org/10.1016/j.gr.2021.07.022.

Hans, K., Joseph, R. (2006). Water in nominally anhydrous minerals. *Reviews in Mineralogy and Geochemistry*, 62, 169-176.

Harigane, Y., Mizukanmi, T., Morishita T., Michibayashi K., Abe, N., & Hirano, N. (2011). Direct evidence for upper mantle structure in the NW Pacific Plate: Microstructural analysis of a petit-spot peridotite xenolith. *Earth and Planetary Science Letters*, 302, 194-202.

Harley, S. L. (1984). An experimental study of the partitioning of Fe and Mg between garnet and orthopyroxene. *Contributions to Mineralogy and Petrology*, 86, 359-373.

Holtzman, B. K., Kohlstedt, D. L., & Zimmerman, M. E. (2003). Melt Segregation and Strain Partitioning: Implications for Seismic Anisotropy and Mantle Flow. *Science*, 301, 1227-1230.

Jung, H., & Karato, S. (2001). Effects of water on dynamically recrystallized grain-size of olivine. *Journal of Structural Geology*, 23, 1337-1344.

Jung, H., Lee, J., & Byeongkwan, K. (2013). Natural type-C olivine fabrics in garnet peridotites in North Qaidam UHP collision belt, NW China. *Tectonophysics*, 594, 91-102.

Jung, H., Mo, M., & Green, H. W. (2009a). Upper mantle seismic anisotropy resulting from pressure-induced slip transition in olivine. *Nature Geoscience*, 73-77.

Jung, H., Mo, M., & Chol, S. H. (2009b). Deformation microstructures of olivine in peridotite from Spitsbergen, Svalbard and implications for seismic anisotropy. *Journal of Metamorphic Geology*, 27, 707-720.

Katayama, I., Jung, H., & Karato, S. (2004). New type of olivine fabric from deformation experiments at modest water content and low stress. *Geology*, 32, 1045-1048.

Katayama, I., & Karato, S. (2006). Effect of temperature on the B- to C-type olivine fabric transition and implication for flow pattern in subduction zones. *Physics of the Earth and Planetary Interiors*, 157, 33-45.

Katayama, I., & Karato, S. (2008). Low-temperature, high-stress deformation of olivine under water-saturated conditions. *Physics of the Earth and Planetary Interiors*, 168, 125-133.

Kohlstedt, D. L., & Mackwell, S. J. (1998). Diffusion of hydrogen and intrinsic point defects in olivine. *Zeitschrift Fur Physikalische Chemie-International Journal of Research in Physical Chemistry & Chemical Physics*, 207, 147-162.

Li, L., Raterron, P., Weidner, D., & Chen, J. H. (2003). Olivine flow mechanisms at 8 Gpa. *Physics of the Earth and Planetary Interiors*, 138, 113-129.

Li, Y. S., Zhang, J. X., Li, S. R., Yu, S. Y., Gong, J. H., & Lin, Y. H. (2013). Metamorphic evolution of the Bashiwake garnet peridotite from the South Altyn Tagh. *Acta Petrologica Sinica*, 29(6), 2073-2092.

Liu, L., Chen, D. L., Zhang, A. D., Sun, Y., Wang, Y., Yang, J. X., & Luo, J. H. (2005). Ultrahigh pressure gneissic K-feldspar garnet clinopyroxenite exsolution in garnet. *Science in China*, 48, 1000-1010.

Liu, L., Kang, L., Cao, Y. T., & Yang, W. Q. (2015). Early Paleozoic granitic magmatism related to the processes from subduction to collision in South Altyn, NW China. *Science China: Earth Sciences*, 58, 1513-1522.

Liu, L., Sun, Y., Xiao, P. X., Che, Z. C., Luo, J. H., Chen, D. L., Wang, Y., Zhang, A. D., Chen, L., & Wang, Y. H. (2002). Discovery of ultrahigh-pressure magnesite-bearing garnet lherzolite (>3.8Gpa) in Altyn Tagh, Northwest China. *Chinese Science Bulletin*, 47, 881-886.

Liu, L., Wang, C., Cao, Y. T. Chen, D. L., Kang, L., Yang, W. Q., & Zhu, X. H. (2012). Geochronology of multi stage metamorphic events: Constraints on episodic zircon growth from the UHP eclogite in the South Altyn, NW China. *Lithos*, 136-139, 10-26.

Liu, L., Zhang, J. F., Cao, Y. T., Green, H., Yang, W. Q., Xu, H. J., Liao, X. Y., & Kang, L. (2018). Evidence of former stishovite in UHP eclogite from the South Altyn Tagh, Western China. *Earth and Planetary Science Letters*, 484, 353-362.

Liu, Y.S. (2011). Guide book for ICPMSDataCal. *China University of Geosciences*, 1–32.

Mackwell, S. J., & Kohlstedt, D. L. (1990). Diffusion of hydrogen in olivine: implications for water in the mantle. *Journal of Geophysical Research*, 95, 5079-5088.

Michibayashi, K., & Mainprice, D. (2004). The role of pre-existing mechanical anisotropy on shear zone development within oceanic mantle lithosphere: an example from the Oman ophiolite. *Journal of Petrology*, 45, 405-414.

Michibayashi, K., Mainprice, D., & Fujii, A. (2016). Natural olivine crystal-fabrics in the western Pacific convergence region: A new method to identify fabric type. *Earth and Planetary Science Letters*, 443, 70-80.

Mizukami, T., Wallis, S.R., & Yamamoto, J. (2004). Natural examples of olivine lattice preferred orientation patterns with a flow normal a-axis maximum. *Nature*, 427, 432–436.

Muramoto, M., Michibayashi, K., Ando, J., & Kagi, H. (2011). Rheological contrast between garnet and clinopyroxene in the mantle wedge: an example from Higashi-akaishi peridotite mass, SW Japan. *Physics of the Earth and Planetary Interiors*, 84, 14-33.

Nickel, K.G. & Green, D.H. (1985). Empirical geothermobarometry for garnet peridotites and implications for the nature of the lithosphere, kimberlites and diamonds. *Earth and Planetary Science Letters*, 73, 158-170

Ohuchi, T., Kawazoe, T., & Nishihara, Y. (2011). High pressure and temperature fabric transitions in olivine and variations in upper mantle seismic anisotropy. *Earth and Planetary Science Letters*, 304, 55-63.

O'Neill, N. H. (1981). The transition between spinel lherzolite and garnet lherzolite, and its use as a Geobarometer. *Contributions to Mineralogy and Petrology*, 77, 185-194.

Park, Y., & Jung H. (2015). Deformation microstructures of olivine and pyroxene in mantle xenoliths in Shanwang, eastern China, near the convergent plate margin, and implications for seismic anisotropy. *International Geology Review*, 57, 629-649.

Paterson, M.S. (1982). The determination of hydroxyl by infrared absorption in quartz, silicate glasses and similar materials. *Bulletin de Mineralogie*, 105, 20-29.

Simakov, S. K., & Taylor, L. A. (2000). Geobarometry for mantle eclogites: solubility of Ca-tschermaks in clinopyroxene. *International geology review*, 42, 534-544.

Skemer, P., Katayama, I., Jiang, Z. T., & Karato, S. (2005). The misorientation index: Development of a new method for calculating the strength of lattice-preferred orientation. *Tectonophysics*, 411, 157-167.

Skemer, P., Katayama, I., & Karato, S. (2006). Deformation fabrics of the Cima di Gagnone peridotite massif, Central Alps, Switzerland: evidence of deformation at low temperatures in the presence of water. *Contributions to Mineralogy and Petrology*, 152, 43–51.

Spear, F.S. (1993). Metamorphic phase equilibria and pressure-temperature-time paths. *Mineralogical Society of America Monograph.*

Sun, S., Dong, Y., Liu, X., He, D., & Cheng, C. (2019). Fabrics, geothermometry, and geochronology of the Songshugou ophiolite: Insights into the tectonic

evolution of the Shangdan suture, Qinling orogen, China. *Lithosphere*, 11(6), 784-803. https://doi.org/10.1130/L1032.1.

Taylor, W. R. (1998). An experimental test of some geothermometer and geobarometer formulations for upper mantle peridotites with application to the thermobarometry of fertile lherzolites and garnet websterite. *Neues Jahrbuch für Mineralogie Abhandlungen*, 172, 381-408.

Tommasi, A., Mainprice, D., Canova, G., & Chastel, Y. (2000). Viscoplastic self-consistent and equilibrium-based modeling of olivine lattice preferred orientations. Implications for upper mantle seismic anisotropy. *Journal of Geophysical Research: Solid Earth*, 105, 7893–7908.

Tommasi, A., Vauchez, A., Godard, M., & Belley, F. (2006). Deformation and melt transport in a highly depleted peridotite massif from the Canadian Cordillera: implications to seismic anisotropy above subduction zones. *Earth and Planetary Science Letters*, 252, 245-259.

Tommasi, A., Vauchez, A., & Ionov, D.A. (2008). Deformation, static recrystallization, and reactive melt transport in shallow subcontinental mantle xenoliths (Tok Cenozoic volcanic field, SE Siberia). *Earth and Planetary Science Letters*, 272, 65-77.

Wang, C., Liu, L., Chen, D. L., & Cao, Y. T. (2011). Petrology, Geochemistry, Geochronology, and Metamorphic Evolution of Garnet Peridotites from South Altyn Tagh UHP Terrane, Northwestern China: Records Related to Crustal Slab Subduction and Exhumation History. *Ultrahigh-Pressure Metamorphism. 25 Years After the Discovery of Coesite and Diamond*, 541-577.

Wang, Q., Ji, S. C., & Xu, Z. Q. (2007). Lattice-Preferred orientation, water content and seismic anisotropy of olivine: Implication for deformation environment of continental subduction zones. *Acta Petrologica Sinica*, 23(12), 3065-3077.

Wang, Q. (2010). A review of water contents and ductile deformation mechanisms of olivine: Implications for the lithosphere–asthenosphere boundary of continents. *Lithos*, 120, 30-41.

Wang, Q., Xia, Q. K., & O'reilly, S. Y. (2013a). Pressure- and stress-induced fabric transition in olivine from peridotites in the Western Gneiss Region (Norway): implications for mantle seismic anisotropy. *Journal of Metamorphic Geology*, 31, 93-111.

Wang, Y., Zhang, J., & Shi, F. (2013b). The origin and geophysical implications of a weak C-type olivine fabric in the Xugou ultrahigh pressure garnet peridotite. *Earth and Planetary Science Letters*, 36, 63-73.

Wu, C. M., & Zhao, G. C. (2011). The applicability of garnet-orthopyroxene geobarometry in mantle xenoliths. *Lithos*, 125 (1-2), 1-9.

Xu, Z. Q., Chen, J., Wang, Q., Zeng, L. S., Yang, J. S., Chen, F. Y., Li, T. F., & Liang, F. H. (2005). Type-C olivine fabric in the Zhimafang garnet peri-

dotite of the Southern Sulu ultrahigh-pressure metamorphic terrane: Formation conditions and tectonic implications. *Acta Petrologica Sinica*, 21(2), 389-397.

Xu, Z. Q., Wang, Q., & Ji, S. C. (2006). Petrofabrics and seismic properties of garnet peridotite from the UHP Sulu terrane (China): Implications for olivine deformation mechanism in a cold and dry subducting continental slab. *Tectonophysics*, 421, 111-127.

Yang, J. J., & Powell, R. (2008). Ultrahigh-pressure garnet peridotites from the devolatilization of sea-floor hydrated ultramafic rocks. *Journal of Metamorphic Geology*, 26, 695-716.

Zhang, J. X., Mattinson, C. G., Meng, F. C., & Wan, Y. S. (2005). An Early Palaeozoic HP/HT granulite-garnet peridotite association in the south Altyn Tagh, NW China: P-T history and U-Pb geochronology. *Journal of Metamorphic Geology*, 23, 491-510.

Zhang, J. X., Mattinson, C. G., Yu, S. Y., & Li, Y. S. (2014). Combined rutile-zircon thermometry and U-Pb geochronology: New constraints on Early Paleozoic HP/UHT granulite in the south Altyn Tagh, north Tibet, China. *Lithos*. 200–201, 241-257.